HHS Public Access

Author manuscript

J Neuroimaging. Author manuscript; available in PMC 2017 September 26.

Published in final edited form as:

J Neuroimaging. 2015 ; 25(5): 799–806. doi:10.1111/jon.12193.

Heterogeneity of Multiple Sclerosis White Matter Lesions Detected With T2*-Weighted Imaging at 7.0 Tesla

Bing Yao, PhD, **Vasiliki N. Ikonomidou, PhD**, **Fredric K. Cantor, MD**, **Joan M. Ohayon, CRNP**, **Jeff Duyn, PhD**, and **Francesca Bagnato, MD, PhD**

Advanced Magnetic Resonance Imaging Section Laboratory of Functional and Molecular Imaging, National Institute of Neurological Disorders and Stroke (NINDS), NIH, Bethesda, MD (BY, JD); Neuroimaging Center, Kessler Foundation, West Orange, NJ (BY); Neuroimmunology Branch (NIB), NINDS, NIH, Bethesda, MD (VNI, FKC, JMO, FB); Department of Bioengineering, Volgenau School of Engineering, George Mason University, Fairfax, VA (VNI); and Neurology Department, University of Maryland, Baltimore, MD (FB)

Abstract

BACKGROUND AND PURPOSE—Postmortem studies in multiple sclerosis (MS) indicate that in some white matter lesions (WM-Ls), iron is detectable with T_2*-weighted (T_2*-w), and its reciprocal R_2* relaxation rate, magnetic resonance imaging (MRI) at 7.0 Tesla (7T). This iron appears as a hyperintense rim in R_2* images surrounding a hypointense core. We describe how this observation relates to clinical/radiological characteristics of patients, in vivo.

METHODS—We imaged 16 MS patients using 3T and 7T scanners. WM-Ls were identified on T_1-w/T_2-w 3T-MRIs. Thereafter, WM-Ls with a rim of elevated R_2* at 7T were counted and compared to their appearance on conventional MRIs.

RESULTS—We counted 36 WM-Ls presenting a rim of elevated R_2* in 10 patients. Twenty-three (64%) lesions coincided with focal WM-Ls on T_2-w MRIs; 13 (36%) coincided with only portions of larger lesions on T_2-w images; and 20 (56%) corresponded to a hypointense chronic black hole. WM-Ls presenting a rim of elevated R_2* were seen in both relapsing-remitting patients with low disability and in those with long-standing secondary progressive MS.

CONCLUSIONS—WM-Ls with a contour of high R_2* are present at different MS stages, potentially representing differences in the contribution of iron in MS disease evolution.

Keywords

Multiple sclerosis; iron; 7.0 tesla; magnetic resonance imaging; T_2*-weighted

Introduction

Several distinct pathological processes subtend the formation of white matter lesions (WM-Ls) in patients with multiple sclerosis (MS).[1] While this pathological heterogeneity has been

Correspondence: Address correspondence to Francesca Bagnato, MD, PhD, Department of Neurology, University of Maryland, 110 S, Paca Street, Baltimore, MD 21201. fbagnato@umm.edu.

Conflicts of Interest: None of the authors has any conflicts with the work.

partially identified postmortem with histology studies,[1] its in vivo characterization with imaging remains limited. The identification of such pathological heterogeneity in vivo could help understand: (1) the mechanisms of disease occurrence and evolution, (2) the basis of patient disability and its degree of reversibility, and (3) medication effect.

The increased magnetic susceptibility contrast achievable with magnetic resonance imaging (MRI) at 7.0 Tesla (7T) provides an opportunity to further characterize WM-L pathology in MS. Recent combined imaging and pathological postmortem studies demonstrated that T_2*-weighted (T_2*-w) multigradient-echo (ME-GRE) MRI at 7T makes it possible to study iron concentration in brain tissue of: (1) human donors who died without neurological illnesses,[2–4] (2) patients with MS,[5–7] and (3) patients who died with non-MS-related neurological conditions.[8,9] Tracking iron in MS is promising because it has the potential to disclose the presence of pathological markers. Microglia in different stages is one of these pathological markers.[5–7,10]

Postmortem imaging studies of MS using T_2*-w 7T MRI and its reciprocal R_2* relaxation rate ($R_2^* = 1/T_2^*$) showed that some WM-Ls and gray matter cortical lesions characteristically present with a rim partly or entirely accentuated by increased R_2* surrounding a core of relatively low R_2*.[5–7] Histopathological analyses have demonstrated that this rim enhancement may reflect the presence of iron trapped within activated microglia.[5–7] There is evidence that this iron may be also associated with dystrophic (senescent) microglia, hence representing a different phase of the disease.[10]

However, it remains unknown how the presence of WM-Ls surrounded by a rim of increased signal on R_2* relates to clinical features of MS patients. It has never been investigated when these types of WM-Ls become visible during the time course of the disease and how they relate to its severity and progression measured by other imaging and clinical metrics.

In this study, we conducted a series of MRIs at both 3T and 7T in 16 patients with MS. The presence or absence of WM-Ls surrounded by a rim of increased R_2* was assessed. Once these lesions were identified on R_2* images, their characterization in relation to WM-Ls seen in T_2-w fast spin echo (FSE), then T_2-w fluid attenuated inversion recovery (FLAIR) images, T_1-w pre- and postcontrast SE images, and cerebrospinal fluid tissue-specific images (CSF-TSI)[11–13] was investigated. CSF-TSI allows visualization of WM-Ls with MRI characteristics suggestive of the presence of CSF-like fluid, and representing lesions with extensive tissue destruction.[12,13] Clinical characteristics of patients in relation to presence of WM-Ls with a hyperintense rim on R_2* images were also analyzed.

Materials and Methods

Study Design and Subjects

The study was performed at the National Institute of Neurological Disorders and Stroke (NINDS), NIH, Bethesda, MD, USA. The Institutional Research Board of the NINDS approved the study (NINDS No. 06-N-154), and each subject provided informed written consent prior to participation. Figure 1 depicts the study design. We included 16 consecutive patients with clinically definite MS[14] and 10 sex- and age-matched healthy volunteers. We

previously reported the study inclusion and exclusion criteria.[15] Each person underwent a 3T MRI (MRI-1) and a 7T MRI (MRI-2) scan obtained 2 weeks apart. In patients only, when a contrast-enhancing lesion (CEL) was noted on MRI-1, postcontrast sequences were obtained at the MRI-2.

The 2-week interval was chosen on the basis of magnet time availability and patients' schedules. Clearly, some disease progression could have occurred in between scans, but we reasoned that such a progression would not affect the type of analysis we were performing with our work. In patients presenting CELs on MRI-1 and/or MRI-2, the 7T scan, inclusive of pre- and post-contrast sequences was repeated 1 month later (MRI-3). On the same day of either MRI-1 or MRI-2, each patient underwent a clinical evaluation, to assess the expanded disability status scale (EDSS) score.[16]

Upon imaging, 1 patient presented no brain lesions on conventional MRI at 3T. Evidence of disease in this patient was present in the spinal cord (data not shown). Brain R_2* MRI at 7T did not show any focal abnormalities either. This patient was therefore removed from subsequent analyses. Table 1 displays demographic, clinical, and imaging characteristics of the 15 patients included in the analysis.

Image Acquisition and Reconstruction

The 3T MRIs were acquired using a General Electric magnet (GE Medical Systems, Milwaukee, WI, USA) equipped with an 8-channel receive-only head array. Pre- and postcontrast T_1-w SE images, noncontrast T_2-w FSE, T_2-w FLAIR, and 3-dimensional magnetization prepared rapid gradient echo (MP-RAGE)-based T_1-w and CSF-TSI were acquired as previously detailed.[11,13,17]

The 7T MRIs were acquired using a whole body GE Signa 7 T MRI scanner (GE Medical Systems) with a 32-channel detector array (Nova Medical, Wilmington, MA, USA). To improve temporal signal stability and compensate for respiration-induced magnetic field changes in the brain,[18] a real-time modulation of B_0 shims (second-order) was carried out. The scanning protocol included 2-dimensional T_2*-w ME-GRE images with 0.31 mm × 0.31 mm^2 in plane resolution, slice thickness = 0.8 mm, slice space = 0.2 mm, repetition time = 2,000 ms, flip angle = 75°, echo times (TEs) = 15.5, 30.0, and 44.5 ms, and bandwidth = 62.5 kHz. Quantitative R_2* and phase maps were then generated by analyzing the signal decay as a function of TE. Details on image acquisition and reconstruction of data were previously described.[15] A 3-dimensional T_1-w MP-RAGE image was also acquired with 1 mm^3 isotropic resolution, flip angle = 9°, TE = 2.8 ms, TR = 5.9 ms, Inversion Time = 1,200 ms, bandwidth = 32 kHz, and 11 minute acquisition time.

In patients previously noted to have CELs on MRI-1 at 3T, the entire 7T protocol was acquired twice, before and after the injection of Gd-DTPA. In these cases, the T_1-w 3-dimensional MP-RAGE was acquired 5 and 40 minutes after the contrast injection. Additionally, these patients underwent two 7T MRIs (MRI-2 and MRI-3) obtained a month apart.

Image Postprocessing and Analysis

Image registration—In each patient, 3T images, ie, T_1-w SE, T_2-w FSE, and T_2-w FLAIR images were registered to the 7T GRE magnitude image using a coregistration algorithm implemented in the statistical parametric mapping software package (SPM8, Wellcome Trust Centre for Neuroimaging, London, UK). The registration involved the following steps. First, the 3T T_1-w SE and T_2-w FLAIR images were registered to the 3T T_2-w SE image. Second, the 3T T_2-w FSE image was registered to the corresponding 7T GRE magnitude image. Third, the translation-rotation matrix obtained in the second step was applied to the images resulting from the first step to generate the final registered image data sets. The 7T R_2* and phase images were inherently coregistered to the magnitude image and thus needed no additional registration. In this way, all the corresponding 3T and 7T images in the same patient were registered. Careful visual inspection was performed after every registration step to ensure successful registration.

CSF-TSI were registered to the same space using the registered FLAIR images as reference. First, white and gray matter TSI images were combined and aligned to FLAIR using an affine transform with 9 degrees of freedom. The obtained transformation matrix was used to register the CSF-TSI image to the T_2-w FLAIR.

Brain parenchymal fraction (BPF)—BPF was measured with the structural imaging evaluation of normalized atrophy (SIENAx) software[19] using the 3- dimensional MP-RAGE images obtained at 3T.

WM-Ls identification—WM-Ls were identified on T_2-w FSE and T_2-w FLAIR images, and T_1-w images obtained before and after Gadolinium injection and on CSF-TSIs.

CELs were identified on postcontrast T_1-w MRIs;[20] ring CELs were defined as presenting a ring-shaped enhancement in at least 1 MRI slice when appearing on multiple slices.[20] On T_1-w SE images obtained before the Gd injection, chronic black holes (cBHs) were defined as any hypointense region corresponding to a hyperintense lesion in T_2-w FSE image, in the absence of acute enhancement;[21] on T_2-w images, lesions were defined in accordance with the Fazekas criteria;[22] on CSF-TSI, lesions were defined as hyperintense area on CSF-TSI corresponding to a cBH on T_1-w SE images.[12,13]

CELs, cBHs, T_2-lesions, and CSF-TSI-lesions were identified by the agreement of 2 investigators (FB and NR for CELs, FB and BY for cBHs and T_2-lesions, and FB and VNI for CSF-TSI-lesions). Two investigators (FB and BY) identified WM-Ls with hyperintense partial or complete rim surrounding a hypointense core on R_2* images.

Results

WM-Ls Surrounded by a Rim of Elevated R_2*

No WM-Ls with increased signal changes in R_2* were seen in the images of any of the healthy subjects. Thirty-six WM-Ls with increased rim signal in R_2* were identified in 10 (67%) patients. None of these 36 lesions corresponded to a CEL on conventional MRI.

Clinical Features of Patients with WM-Ls Surrounded by a Rim of Elevated R_2*

Tables 2 and 3 depict the demographic, clinical, and imaging characteristics of each of the 10 patients presenting WM-Ls contoured by increased signal in R_2*. Due to the small number of patients in each group, (ie, 10 patients had WMLs contoured by increased signal in R_2* and 6 did not) no formal statistics were performed. Results are provided in a descriptive manner. As seen in Table 2, WM-Ls with increased rim signal changes in R_2* were seen either in patients at the early stage of MS and with a low level of disability accumulation or in those with longstanding and advanced secondary progressive MS. Similarly, when looking at the imaging metrics of disease progression on conventional scans reported in Table 3, we observed that WM-Ls with a rim of elevated R_2* were present in patients with a small lesion volume in T_2-w images and virtually no cBHs or CSF-TSI lesions as well as in those patients with larger disease burden in T_1-w, T_2-w, and CSF-TSI or a relatively advanced brain loss.

Radiological Features of WM-Ls Surrounded by a Rim of Elevated R_2* Displays 2 Main Patterns

Twenty-three (64%) WM-Ls contoured by increased R_2* entirely coincided with focal WM-Ls in conventional T_2-w SE and T_2-w FLAIR MRI. Figure 2 shows an example of such a lesion type. The lesion is visible in the magnitude image (Fig 2A). In R_2* the lesion shows an incomplete bright rim (Fig 2B) which in this case corresponded to a dark signal in the phase map (Fig 2C). The lesion entirely coincided with a WM-L in conventional T_2 w images (Figs 2D, 2E) and cBH in T_1-w SE image (Fig 2F).

WM-Ls contoured by increased R_2* appeared to be only a small portion of larger confluent lesions in T_2-w SE and T_2-w FLAIR images in 13 (36%) WM-Ls. Figure 3 shows an example of such lesion type. In this example a rim WM-L was seen in magnitude (Fig 3A) and R_2* images (Fig 3B). Portions of the rim with elevated R_2* was visible in the phase images (Fig 3C). The rim of increased R_2* surrounded a central core of decreased R_2*. This core was only part of a larger lesion on T_2-w SE images and T_2-w FLAIR (Figs 3D, 3E), but coincided with a cBH in both T_2-w FLAIR and T_1-w SE images (Figs 3E, 3F).

Overall, 20 (56%) WM-Ls contoured by increased R_2* were associated with the presence of a cBH and 9 (25%) were associated with the presence of a lesion on CSF-TSI.

Separate Analysis of CELs and WM-Ls with Rim of Elevated R_2*

CELs were seen only in 1 patient. In this patient, we initially observed an active lesion (CEL-1) in the first scan at 3T (MRI-1; image not shown). Postcontrast scans were therefore obtained with the 7T MRI (MRI-2). Five minutes after contrast injection, this CEL presented a patchy enhancement (Fig 4A). This patchy enhancement became more uniformly distributed in a nodular fashion in the T_1-w MPRAGE obtained 40 minutes postcontrast injection (Fig 4B). The R_2* and phase maps obtained at the same time, showed the central core of the enhancing lesion to have decreased R_2* (Fig 4C) and paramagnetic phase shift (Fig 4D). The CEL was no longer enhancing in the follow-up 7T scan (MRI-3) obtained a month apart (image not shown). No clear signal alterations ascribable to the prior presence of that CEL could be unambiguously identified in the R_2* map MRI-3 (Fig 4E). Transient

increased R_2* signal was seen in the vicinity of the lesion. A residual smaller area with paramagnetic phase shift was visible in the phase map (Fig 4F), possibly indicating demyelination.

In the follow-up 7T MRI scan (MRI-3), a new CEL (CEL-2) was identified. This CEL presented a ring-enhancing pattern in the T1-w MPRAGE obtained 5 minutes (Fig 4G) and 40 minutes postcontrast injection (Fig 4H). The ring-enhancing contour coincided with a rim of elevated R_2* (Fig 4I) and a paramagnetic phase shift (Fig 4L). None of these signal alterations were clearly and unambiguously present prior to the enhancement as shown in the MRI obtained a month before its occurrence in Figure 4M and 4N.

Discussion

The results of our work suggest that WM-Ls surrounded by a rim of elevated R_2*, tentatively attributed to increased iron deposition, may be present at various stages of MS. Although seen in a small cohort of 10 cases, these patients presented heterogeneous disease characteristics. Some of them only had a few years of relapsing-remitting MS and demonstrated low level of physical disability; others were in the stage of advanced and long-standing secondary progressive MS. The heterogeneity of our clinical findings is paralleled by the heterogeneity of the radiological evidence, which showed a high degree of the diversity in appearance of WM-Ls contoured by increased R_2* in conventional MRI sequences.

Our study cohort was mainly formed by patients with non active disease by MRI. Therefore, we mostly report data on how WM-Ls surrounded by a rim of elevated R_2* relate to chronic lesions on T_1-w and T_2-w sequences. In this setting, the majority of WM-Ls surrounded by a rim of elevated R_2* entirely coincided with focal nonactive lesions in T_2-w FSE and FLAIR MRIs. About a third of WM-Ls with a rim of increased R_2* were instead only a portion of a larger lesion in T_2-w images. A subset of WM-Ls contoured by increased R_2* also coincided with the presence of pathologically more severe lesions such as cBHs on T_1-w MRI and lesions in CSF-TSI.

Several possible explanations, not necessarily mutually exclusive, may be inferred from our findings. First, one may argue that this in vivo pattern of WM-Ls contoured by increased R_2* closely resembles the one observed in our previously reported postmortem work.[5] In that setting, the core of chronic WM-Ls showed a relatively low R_2* and corresponded to areas of absent myelin and low or absent iron. Increased R_2* around the demyelinated core of these WM-Ls almost invariably matched with iron and ferritin accumulation. Such an accumulation was seen in conjunction with high CD68 immunoreactivity expressed in cells the morphology of which, ie, branched and bipolar, appeared to be that of activated microglia.[5] This type of pathological pattern is the hallmark of slowly expanding lesions.[23] Second, it must be considered that also degradation of dystrophic microglia at MS lesions' edge may lead to a wave of accelerated iron release. This iron may in turn accumulate within other microglia, astrocytes, or axons. If not properly eliminated, it will eventually lead to neurodegeneration.[24,25] The contour of elevated R_2* may still testify the presence of iron within microglia. However, rather than continuous expanding lesional activity, it may

represent the attempt of the microglia to eliminate toxic liberated iron, which would otherwise induce oxidative stress.[25] Clearly, the ultimate and unambiguous explanation of our results would require biopsy and histopathology of one of these lesions in the brain of MS patients in vivo. Demonstrating lesion expansion or stability over time on a lesion-by-lesion basis by longitudinal in vivo MRIs would be another way to establish the presence of slowly expanding activity.

As only a low number ($n = 2$) of CELs (ie, lesions classically regarded as acute) was found, only very preliminary and tentative interpretation can be speculated. One of these CELs appeared as nodular CEL in T_1-w postcontrast MRI. The enhancing core of this active lesion exhibited a decrease in R_2* and paramagnetic phase shift. The initial increase in R_2* surrounding the core of the lesion may reflect the presence of iron associated with severe blood brain barrier damage during the active phase of lesion formation, leading to iron liberation from destroyed oligodendrocytes.[10] A second CEL presented as ring CEL. The ring-enhancing contour seen in T_1-w postcontrast images upon early (ie, 5 minutes) and delay (ie, 40 minutes) acquisition coincided with a ring of increased R_2* and paramagnetic phase shift. Such signal changes were likely not visible in the R_2* and phase maps obtained a month earlier, indicating that they were for the most part temporally coincident with the onset time of contrast uptake. Our findings seem to demonstrate that at least in our case, the ring enhancement may indeed correspond to a ring of iron accumulation. Of note, however, the R_2* image obtained a month prior showed trace of hyperintense signal in the lesion area. Although possibly artifactual, this hyperintensity may signify subtle iron deposits associated with an early blood brain barrier disruption. Blood brain barrier breakdown and some inflammation is indeed known to occur some time prior to manifestation of a CEL.[26,27]

In interpreting our results on both chronic and active WM-Ls, one should also bear in mind that iron deposition is only 1 factor among several that could generate increased signal in $R2^*$ maps.[15,28–30] Increased myelin content due to remyelination may affect changes in R2* via 2 mechanisms. First, remyelinating oligodendrocytes are known to have an elevated content of iron.[31] Second, differences in architectural organization in local regions with undergoing remyelination are also known to be another potential source of signal change in R2* images.[15,28–30] Fiber bundles orientation to the MRI magnetic field (B_0)[31] is also a contributor of R2* changes, although likely minor in our case, where lesions were spatially disseminated.

In conclusion, our current results, although derived from a small cohort of patients, provide a respectable in vivo evidence of the heterogeneity of the pathological processes the contour of elevated R_2* may represent in MS. Studies in larger cohorts of patients are warranted to provide more insight into our preliminary demonstration.

Acknowledgments

The study was supported by the Intramural program of the NINDS-NIH, Bethesda, MD, USA.

References

1. Lassmann H. The pathologic substrate of magnetic resonance alterations in multiple sclerosis. Neuroimag Clin N Am. 2008; 18:563–576.
2. Yao B, Li TQ, Gelderen P, et al. Susceptibility contrast in high field MRI of human brain as a function of tissue iron content. NeuroImage. 2009; 44:1259–1266. [PubMed: 19027861]
3. Shmueli K, de Zwart JA, van Gelderen P, et al. Magnetic susceptibility mapping of brain tissue in vivo using MRI phase data. Magn Reson Med. 2009; 62:1510–1522. [PubMed: 19859937]
4. Fukunaga M, Li TQ, van Gelderen P, et al. Layer-specific variation of iron content in cerebral cortex as a source of MRI contrast. Proc Natl Acad Sci USA. 2010; 107:3834–3839. [PubMed: 20133720]
5. Bagnato F, Hametner S, Yao B, et al. Tracking iron in multiple sclerosis: a combined imaging and histopathological study a 7 tesla. Brain. 2011; 134:3602–3615. [PubMed: 22171355]
6. Pitt D, Boster A, Pei W, et al. Imaging cortical lesions in multiple sclerosis with ultra-high-field magnetic resonance imaging. Arch Neurol. 2010; 67:812–818. [PubMed: 20625086]
7. Mehta V, Pei W, Yang G, et al. Iron is a sensitive biomarker for inflammation in multiple sclerosis lesions. PLoS One. 2013; 8:e57573, 1–11. [PubMed: 23516409]
8. House MJ, St Pierre TG, Kowdley KV, et al. Correlations of proton transverse relaxation rates (R2) with iron concentrations in post mortem brain tissue from Alzheimer disease patients. Magn Reson Med. 2007; 57:172–178. [PubMed: 17191232]
9. Kwan JY, Jeong SY, Van Gelderen P, et al. Iron accumulation in deep cortical layers accounts for MRI signal abnormalities in ALS: correlating 7 tesla MRI and pathology. PLoS One. 2012; 7:e35241. [PubMed: 22529995]
10. Hametner S, Wimmer I, Haider L, et al. Iron and neurodegeneration in the multiple sclerosis brain. Ann Neurol. 2013; Epub ahead of print. doi: 10.1002/ana.23974
11. Ikonomidou VN, van Gelderen P, de Zwart JA, et al. Optimizing brain tissue contrast with EPI: a simulated annealing approach. Magn Reson Med. 2005; 54:373–385. [PubMed: 16032676]
12. Riva M, Ikonomidou VN, Ostuni JJ, et al. Tissue-specific imaging is a robust methodology to differentiate *in vivo* T1 black holes with advanced multiple sclerosis-induced damage. Am J Neuroradiol. 2009; 30:1394–1401. [PubMed: 19406765]
13. Bagnato F, Ikonomidou VN, van Gelderen P, et al. Lesions by tissue specific imaging characterize multiple sclerosis patients with more advanced disease. Mult Scler. 2011; 7:1424–1431.
14. Polman CH, Reingold SC, Edan G, et al. Diagnostic criteria for multiple sclerosis: 2005 revisions to the “McDonald Criteria. Ann Neurol. 2005; 58:840–846. [PubMed: 16283615]
15. Yao B, Bagnato F, Mitsura E, et al. Chronic multiple sclerosis lesions: characterization with high-field-strength MR imaging. Radiology. 2012; 262:206–215. [PubMed: 22084205]
16. Kurtzke JF. Rating neurologic impairment in multiple sclerosis: an expanded disability status scale (EDSS). Neurology. 1983; 33:1444–1452. [PubMed: 6685237]
17. Pellicano C, Gallo A, Li X, et al. Relationship of cortical atrophy to fatigue in patients with multiple sclerosis. Arch Neurol. 2010; 67:447–453. [PubMed: 20385911]
18. van Gelderen P, de Zwart JA, Starewicz P, et al. Real-time shimming to compensate for respiration-induced B0 fluctuations. Magn Reson Med. 2007; 57:362–368. [PubMed: 17260378]
19. Smith SM, Zhang Y, Jenkinson M, et al. Accurate, robust, and automated longitudinal and cross-sectional brain change analysis. NeuroImage. 2002; 17:479–489. [PubMed: 12482100]
20. Davis M, Auh S, Riva M, et al. Ring and nodular multiple sclerosis lesions: a retrospective natural history study. Neurology. 2010; 74:851–856. [PubMed: 20211910]
21. Bagnato F, Jeffries N, Richert ND, et al. Evolution of T1 black holes in patients with multiple sclerosis imaged monthly for 4 years. Brain. 2003; 126:1782–1789. [PubMed: 12821527]
22. Fazekas F, Barkhof F, Filippi M. Unenhanced and enhanced magnetic resonance imaging in the diagnosis of multiple sclerosis. J Neurol Neurosurg Psychiatry. 1998; 64(Suppl 1):2–5. [PubMed: 9436717]
23. Prineas JW, Kwon EE, Cho ES, et al. Immunopathology of secondary-progressive multiple sclerosis. Ann Neurol. 2001; 50:646–657. [PubMed: 11706971]

24. Streit WJ, Braak H, Xue QS, et al. Dystrophic (senescent) rather than activated microglial cells are associated with tau pathology and likely precede neurodegeneration in Alzheimer's disease. Acta Neuropathol. 2009; 118:475–485. [PubMed: 19513731]
25. Haider L, Fischer MT, Frischer JM, et al. Oxidative damage in multiple sclerosis lesions. Brain. 2011; 134:1914–1924. DOI: 10.1093/brain/awr128 [PubMed: 21653539]
26. Silver NC, Lai M, Symms MR, et al. Serial magnetization transfer imaging to characterize the early evolution of new MS lesions. Neurology. 1998; 51:758–764. [PubMed: 9748023]
27. Wuerfel J, Bellmann-Strobl J, Brunecker P, et al. Changes in cerebral perfusion precede plaque formation in multiple sclerosis: a longitudinal perfusion MRI study. Brain. 2004; 127:111–119. [PubMed: 14570816]
28. Lee J, Shmueli K, Kang BT, et al. The contribution of myelin to magnetic susceptibility-weighted contrasts in high-field MRI of the brain. NeuroImage. 2012; 59:3967–3975. [PubMed: 22056461]
29. Oh SH, Kim YB, Cho ZH, et al. Origin of B0 orientation dependent R2(*) (= 1/T2(*)) in white matter. NeuroImage. 2013; 73:71–79. [PubMed: 23376494]
30. Sati P, Silva AC, vanGeldern P, et al. In vivo quantification of T_2 anisotropy in white matter fibers in marmoset monkeys. NeuroImage. 2012; 59:979–985. [PubMed: 21906687]
31. Connor JR, Menzies SL. Relationship of iron to oligodendrocytes and myelination. Glia. 1996; 17:83–93. [PubMed: 8776576]

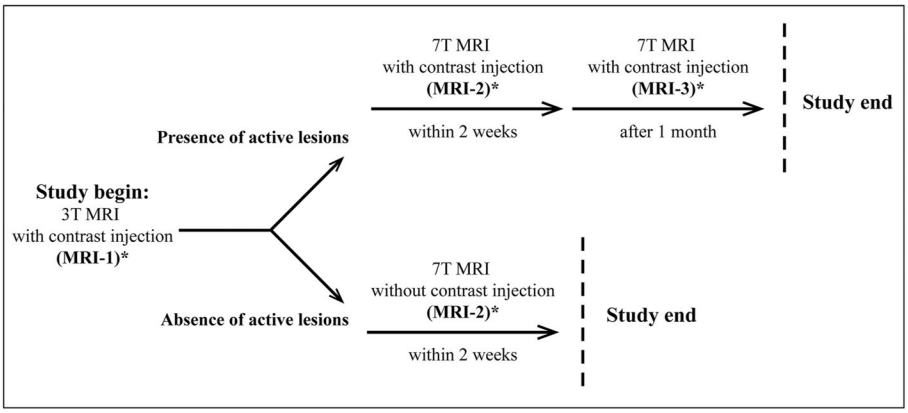

Fig. 1.

Study design. Each person underwent a 3T (MRI-1) and a 7T MRI (MRI-2) scan obtained 2 weeks apart. In patients only, when a CEL was noted in postcontrast imaging of MRI-1, postcontrast sequences were obtained at the MRI-2 7T scan. The 7T scan, inclusive of pre- and postcontrast sequences, was also repeated a month later (MRI-3). On the same day of either MRI-1 or MRI-2, each patient underwent a clinical assessment to establish the EDSS score.

* Indicates the time when the clinical assessment was performed. See text for detailed explanation.

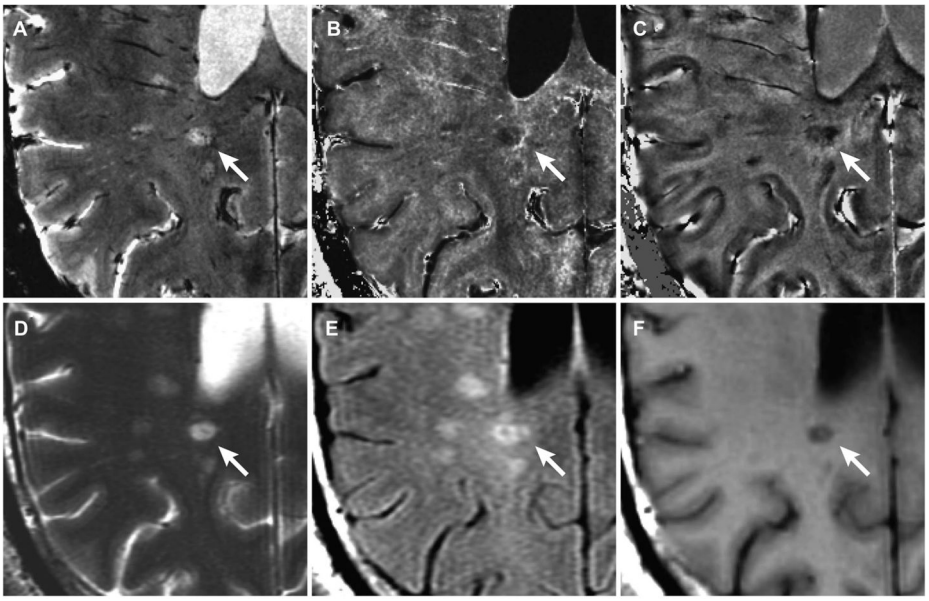

Fig. 2.

WM-L with a rim of increased signal in R_2*. WM-L with a rim of increased signal in R_2* (white arrow) identified in magnitude (A), R_2* (B), and phase (C) map in a RRMS patient with 1.5 years of MS and EDSS score of 2.5 (patient-2 in Tables 2 and 3). The lesion entirely coincides with a focal lesion in T2-w FSE (D), T2-w FLAIR (E) image, and T1-cBH in T1-w SE image (F) at 3T.

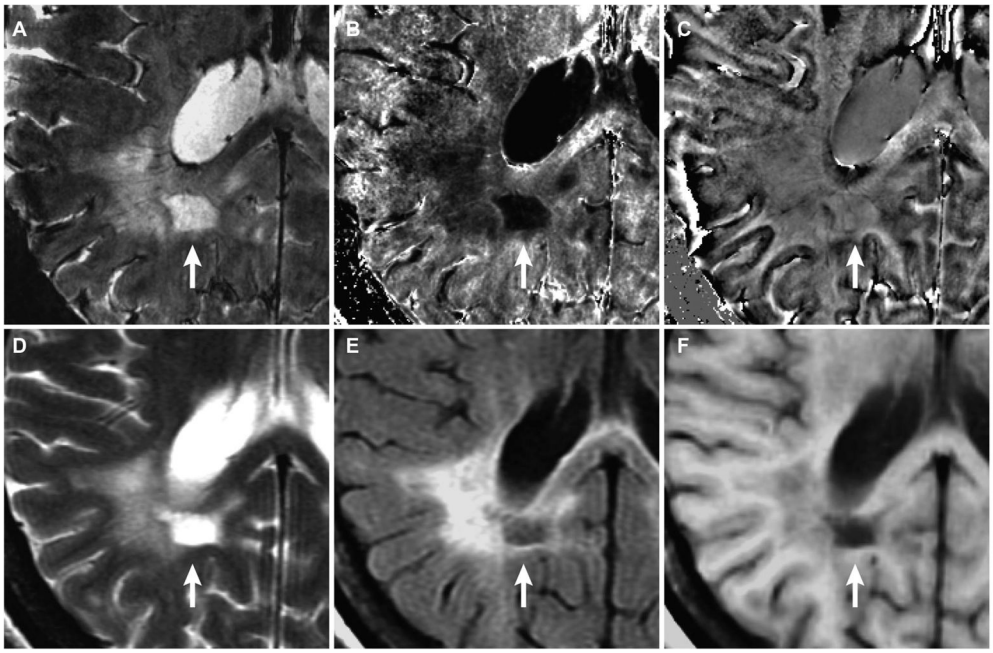

Fig. 3.

WM-L with a rim of increased signal in R_2* WM-L with a rim of increased signal in R_2* (white arrow) identified in magnitude (A), R_2* (B), and phase (C) map in a SPMS patient with 33 years of disease and EDSS score of 6.0 (patient-5 in Tables 2 and 3). The lesion is only part of a larger lesion seen in T2-w FSE (D), T2-w FLAIR (E) image, and T1-w SE (F) image. The lesion also corresponds with a black hole on FLAIR image, indicating end-stage cavitation.

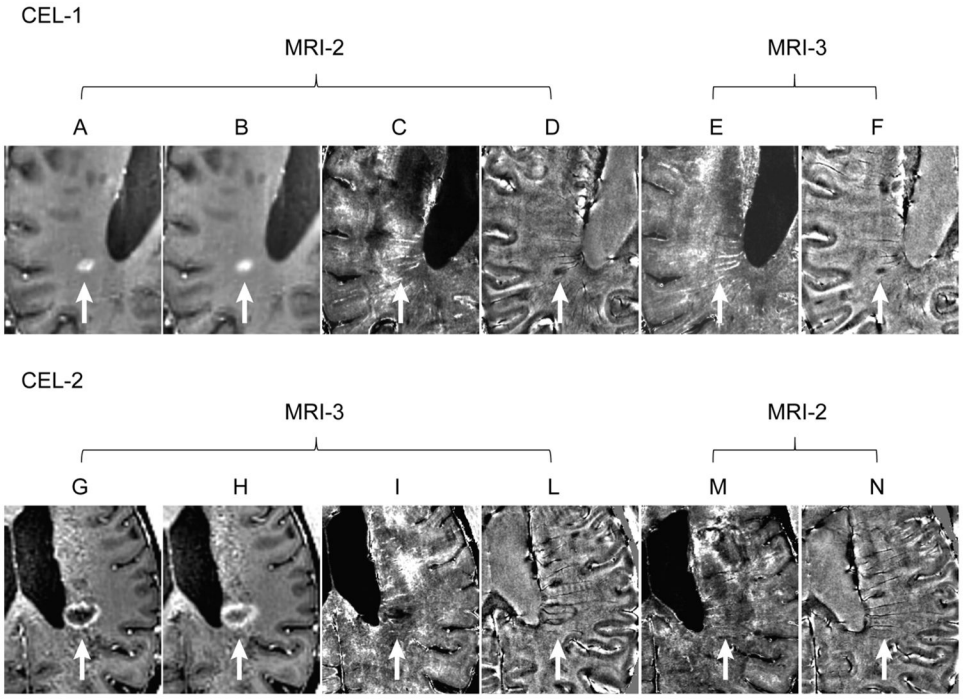

Fig. 4.

Active lesions with and without a rim of elevated R_2 CEL-1 (white arrow) seen in the T1-w MPRAGE of MRI-1 obtained 5 minutes post-Gd injection (A) and 40 minutes post-Gd injection (B). The R_2* and phase maps show the central core of the enhancing lesion had an decreased R_2* (C) and a reduced phase (ie, paramagnetic shift) (D). No clear signal alterations ascribable to the prior presence of that CEL could be unambiguously identified in the R_2* map of MRI-3 (E) obtained a month later when the CEL was no longer enhancing. Residual smaller area with a paramagnetic phase shift was visible in the phase map (F) of MRI-2. CEL-2 in MRI-3 is indicated with white arrow. This CEL presented with a ring-enhancing pattern in the T1-w MPRAGE obtained 5 minutes (G) 40 minutes post-Gd injection (H). The ring-enhancing contour coincided with a rim of elevated R_2* signal (I) and paramagnetic phase shift (L). Minimal signs of signal alterations corresponding to the presence of this lesion were present in the R_2* (M) but not on the phase (N) images obtained a month earlier. The fainting nature of this signal may signify an artifact. One cannot, however, unambiguously exclude minimal brain barrier leakage and iron deposition associated with it. These data were derived from a patient with RRMS, 7.5 years of disease and EDSS score of 2.5 (patient-8 in Tables 2 and 3).

Table 1

Demographic, Clinical and Imaging Characteristics of the Study Cohort

	Patients (*n* = 15)	Healthy Volunteers (*n* = 10)	*P*-Value
Age	44.8 ± 8.8 (28–57)	44.3 ± 11.1 (22–57)	.9*
Sex (female/male)	7/8	6/4	.5**
Years of MS	11.3 ± 10.1 (.3–33)	N/A	N/A
MS type (RR/SP)	13/2	N/A	N/A
EDSS	1.5 (0–6.0)	N/A	N/A
T_2-LV (cm^3)	8.9 ± 13.1 (0–42.5)	N/A	N/A
cBH-LV (cm^3)	3.9 ± 6.3 (0–18.4)	N/A	N/A
CSF-TSI-LV (cm^3)	1.2 ± 2.6 (0–7.3)	N/A	N/A
BPF	.74 ±.05 (.67–.83)	N/A	N/A

Data related to continuous variables are expressed in mean ± SD (minimum-maximum value), but for the expanded disability stats scale (EDSS) score for which median (minimum-maximum values) are provided; N/A = not applicable;

* by unpaired *t*-test;

** by x-2 test.

RR = relapsing remitting; SP = secondary progressive; T_2-LV = volume of hyperintense lesions in T_2-w image; cBH-LV = chronic black holes lesion volume; CSF-TSI-LV = volume of hyperintense lesions in cerebrospinal fluid tissue-specific imaging; BPF = brain parenchyma fraction.

Table 2

Demographic and Clinical Features of Patients with WM-Ls with a Rim of elevated R_2*

	Age	Sex	MS Years	MS Type	EDSS	Disease Modifying Therapy
Pt-1	40	Male	.9	RRMS	1.0	None
Pt-2	40	Male	1.5	RRMS	2.5	Interferon beta-1a
Pt-3	56	Male	25	RRMS	1.5	Interferon beta-1b
Pt-4	44	Female	15	RRMS	1.0	Interferon beta-1a
Pt-5	57	Female	33	SPMS	6.0	None
Pt-6	30	Female	1.1	RRMS	1.5	Interferon beta-1b
Pt-7	49	Female	20.1	RRMS	4.0	Daclizumab
Pt-8	40	Male	7.5	RRMS	2.5	Monthly methylprednisolone
Pt-9	49.5	Male	21.7	RRMS	2.0	Daclizumab
Pt-10	38	Male	6	RRMS	1.0	Interferon beta-1b

EDSS = expanded disability stats scale; RR = relapsing remitting; SP = secondary progressive.

Table 3

MRI Features of Patients with WM-Ls with a Rim of Elevated R_2*

	T_2-LV (cm^3)	cBH-LV (cm^3)	CSF-TSI-LV (cm^3)	BPF
Pt-1	1.1	.2	0	.83
Pt-2	3.6	2.1	.5	.86
Pt-3	6.6	3.8	.5	.69
Pt-4	.5	.4	0	.81
Pt-5	45.5	16.8	6.6	.71
Pt-6	.5	.1	0	.81
Pt-7	30.1	18.4	7.3	.67
Pt-8	11.2	2.7	.7	.75
Pt-9	8.7	3.0	Not obtained	.71
Pt-10	5.5	.4	0	.71

T_2-LV = volume of hyperintense lesions in T_2-w image; cBH-LV = chronic black holes lesion volume; CSF-TSI-LV = volume of hyperintense lesions in cerebrospinal fluid tissue-specific imaging; BPF = brain parenchyma fraction.